Weighing the Local Interstellar Medium Using Gamma Rays and Dust

Axel Widmark,[1,*] Michael Korsmeier,[2,†] and Tim Linden[2,‡]
[1]Dark Cosmology Centre, Niels Bohr Institute, University of Copenhagen, Jagtvej 128, 2200 Copenhagen N, Denmark
[2]Stockholm University and The Oskar Klein Centre for Cosmoparticle Physics, Alba Nova, 10691 Stockholm, Sweden

(Received 11 September 2022; revised 24 January 2023; accepted 16 March 2023; published 19 April 2023)

Cold gas forms a significant mass fraction of the Milky Way disk, but is its most uncertain baryonic component. The density and distribution of cold gas is of critical importance for Milky Way dynamics, as well as models of stellar and galactic evolution. Previous studies have used correlations between gas and dust to obtain high-resolution measurements of cold gas, but with large normalization uncertainties. We present a novel approach that uses Fermi-LAT γ-ray data to measure the total gas density, achieving a similar precision as previous works, but with independent systematic uncertainties. Notably, our results have sufficient precision to probe the range of results obtained by current world-leading experiments.

DOI: 10.1103/PhysRevLett.130.161002

Measuring the gas content of the Milky Way and local universe is crucial for many fields in astronomy. Cold gas is the most uncertain baryonic component in Milky Way mass models, hampering the precision of dynamical mass measurements of dark matter [1,2]. It is also essential for our theoretical understanding of star and galaxy formation [3,4].

The dominant gas species of the interstellar medium (ISM) are atomic and molecular hydrogen (HI and H_2), where especially the latter is difficult to observe directly as it lacks a permanent electric dipole moment. CO observations are often used as a tracer [5]. However, the CO-to-H_2 ratio is uncertain and depends on the temperature and density of their environment [6]. A significant fraction of H_2 is known to be CO dark, but the precise amount is poorly constrained [7–10].

Gas is additionally traced by dust [11], which is typically easier to observe and serves as a useful proxy for a galaxy's gas content [12–17]. Dust is also of direct physical importance for a number of complex thermal and chemical processes of the ISM, affecting star and planet formation [18]. In the Milky Way, the dust-to-gas ratio has been estimated using gas observations coming from stellar sight-line UV absorption [19–21], soft x-ray scattering [22], or 21 cm emission [23–25] (see Supplemental Material [26], Appendix A for further details).

In this Letter, we develop a novel method for measuring the local Milky Way gas content, within roughly 2 kpc, using γ-ray data from the Fermi-LAT telescope. The diffuse γ-ray flux is produced primarily by the hadronic interactions of cosmic rays (CRs) with interstellar gas. Because CR measurements (e.g., by AMS-02) strongly constrain the local cosmic-ray density, γ-ray measurements can, in turn, be used to strongly constrain the gas density. Importantly, the hadronic interactions that produce γ-ray emission are entirely agnostic as to the temperature, spin, or ionization state of the gas targets, making our gas density calculations highly complementary to the techniques described above. Furthermore, we use a new dust map [83] that was recently produced from observations by the astrometric *Gaia* mission [84], and has the novel quality of being three

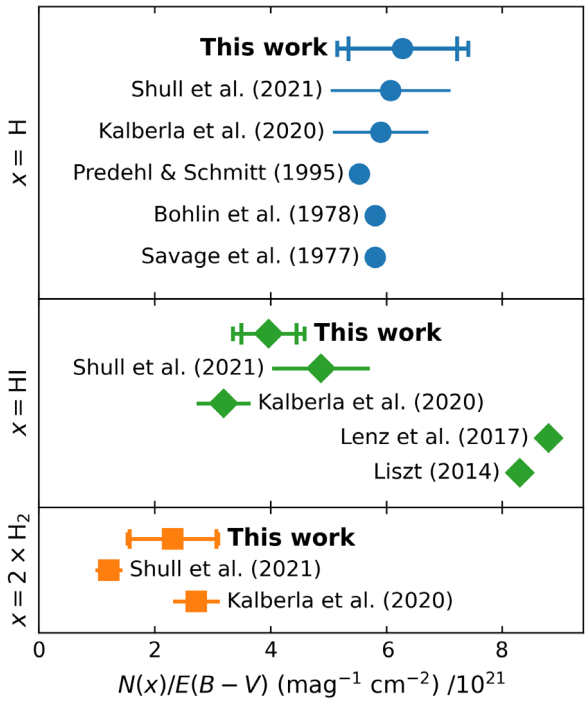

FIG. 1. Ratio between $E(B-V)$ dust reddening and gas, as determined by our γ-ray analysis. The three panels depict total hydrogen (H), and its atomic (HI) and molecular (H_2) species. The inner error bars of our results correspond to the uncertainty of our fit, while the outer errors bars include a 10% systematic uncertainty on the γ-ray cross sections added in quadrature. Our results are consistent with Refs. [19,20,22,25], but in tension with Refs. [23,24].

dimensional and (unlike most previous studies) observed in the optical rather than the far infrared.

Figure 1 shows the main results of our study. Our measurements of the dust-to-gas ratio have a similar precision as previous work, but are affected by an independent set of systematic uncertainties. Excitingly, our results are precise enough to probe the range of results from state-of-the-art measurements. Furthermore, our study produces a novel and accurate model for high-latitude diffuse γ-ray emission from the Milky Way [85], with many applications to studies of extragalactic γ-ray emission and extended γ-ray sources.

γ-ray emission models.—γ rays provide a unique probe into galactic gas. Here, we focus on 0.1–100 GeV γ rays observed at high Galactic latitudes. These are created by several processes, including the interaction of CRs with gas [86,87]. The most important process is π^0 production from hadronic interactions, while the bremsstrahlung of CR electrons provides a $\mathcal{O}(10\%)$ contribution below a few GeV [88–92].

The γ-ray flux produced from a CR component i and a gas component j is given by the integration of the γ-ray emission per interaction ϵ^{ij} and the number density of the gas component ρ_j along the line of sight (LOS) in the direction l, b (longitude, latitude):

$$\frac{d^2\phi_\gamma^{ij}}{d\Omega dE_\gamma}(E_\gamma, l, b) = \int_{\mathrm{LOS}} d\ell \rho_j(\boldsymbol{x}) \epsilon^{ij}(E_\gamma, \boldsymbol{x}), \quad (1)$$

where the emission per interaction is given by convolving the CR flux ϕ_{CR}^i with the γ-ray production cross section $\sigma_{ij\to\gamma}$:

$$\epsilon^{ij}(E_\gamma, \boldsymbol{x}) = \int dE_i \frac{d\phi_{\mathrm{CR}}^i}{dE_i}(E_i, \boldsymbol{x}) \frac{d\sigma_{ij\to\gamma}}{dE_\gamma}(E_i, E_\gamma). \quad (2)$$

The product $\rho_j(\boldsymbol{x})\epsilon^{ij}(E_\gamma, \boldsymbol{x})$ is commonly called γ-ray emissivity. Thus, the flux depends on the CR flux and the total gas density. Importantly, the γ-ray flux is essentially unaffected by whether the gas is cold or hot, molecular or atomic, ionized or neutral. The dominant CR fluxes are protons and helium, while contributions from heavier nuclei are subdominant. The flux of electrons and positrons is also suppressed compared to protons by 2–3 orders of magnitude, but is important for low-energy bremsstrahlung due to its faster cooling timescale and for the inverse Compton emission.

We employ the propagation model recently explored in Ref. [93] and refit it to the CR data of p, He, ^{3}He/^{4}He, $\bar{p}/p$, and e^+ provided by AMS-02. The e^- data is adjusted in a postprocedure. The CR model includes diffusion, convection, continuous energy losses, and fragmentation losses. Our model is based on the GALPROP code [94], which numerically solves the propagation equations. It includes several improvements compared to previous studies. Details are described in the Supplemental Material [26], Appendix B.

Besides CR-gas interactions, we model the following processes: (1) Galactic and extragalactic γ-ray point sources [95]; (2) the emission from inverse Compton scattering (ICS), i.e., the up-scattering of low-energy photons by CR electrons and positrons; and (3) an isotropic emission that stems from faint and unresolved extragalactic point sources, charged CR contamination, and residual Galactic emission.

We perform template fits to the Fermi-LAT data constraining the number of γ-ray photons attributed to each process or gas tracer as sketched in Fig. 2. Ultimately, we obtain the conversion factor from the gas tracers (21 cm, dust, CO) to the gas densities (H, HI, H_2). The gas tracers and the exact fitting procedure are explained below.

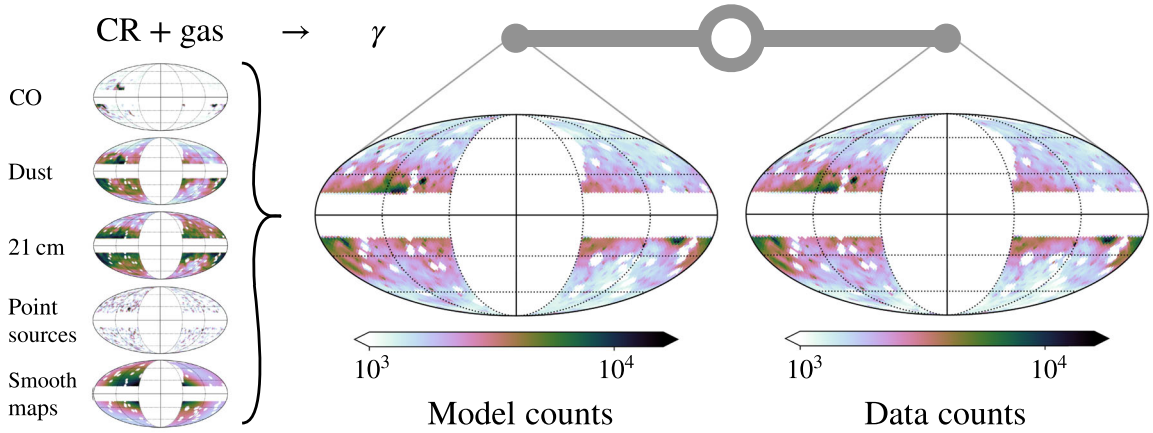

FIG. 2. γ rays are produced by the interaction of CRs with gas, as well as a few other processes like inverse Compton emission or point sources. We perform a template fit of the local γ-ray sky by comparing model counts and Fermi-LAT data. We note that maps are corrected for the Fermi-LAT instrumental exposure, which varies across the sky. We use cuts of $|l| < 60°$ to avoid the Galactic center and the Fermi bubbles, and $|b| < 16°$ to select nearby emission sources. From the normalization of each template, we infer the conversion factors of the gas tracers to gas densities, most notably, from dust reddening to cold hydrogen gas.

Gas tracers.—The ISM is separated into distinct gas phases, broadly divided into a cold and warm neutral medium (CNM and WNM) [4,96–98]. The different gas components and species are traced by different maps in our model:

CO: Very cold molecular gas is traced by radio observations of rotational modes in carbon monoxide (CO). We use the two-dimensional full-sky CO data from the Planck survey (the "Type 2" map from Ref. [99]). Canonically, the conversion factor between the CO $J = 1 \to 0$ transition signal and the H_2 column density is equal to $(2 \pm 0.6) \times 10^{20}\ \mathrm{cm^{-2}\,K^{-1}\,km^{-1}\,s}$ [6,100]. The component of CO-traced H_2 has a small scale height, and thus, due to our cut on Galactic latitude, its relative contribution is small.

Dust: We use a three-dimensional dust map to trace molecular and atomic hydrogen in the CNM. This dust map was produced using *Gaia* data [83], given in terms of extinction per distance in units $\mathrm{mag\,pc^{-1}}$, at a wavelength of 6500 Å (corresponding to the center of *Gaia*'s photometric G band); this extinction is proportional to $E(B-V)$ by a factor of $0.88 \times 3.1 = 2.73$ [83,101]. The conversion factor between $E(B-V)$ dust reddening and the hydrogen nuclei column density is roughly $6 \times 10^{21}\ \mathrm{mag^{-1}\,cm^{-2}}$, although the precise value is highly uncertain (see Fig. 1). The dust distribution of this map has a small scale height. Most of it is contained within 100 pc from the midplane, with only weak tails to heights around 300 pc. Hence it is inconsistent with the ∼400 pc scale height of the WNM, and we make the interpretation that this dust map only traces the CNM.

21 cm: We use the two-dimensional full sky 21 cm map called HI4PI [102], integrated over LOS velocities between $(-90, 90)\ \mathrm{km\,s^{-1}}$, to trace atomic hydrogen in the CNM and WNM. This map overlaps with the dust map, since both trace CNM HI. Canonically, the conversion factor between the 21 cm signal and the HI column density is equal to $1.823 \times 10^{18}\ \mathrm{cm^{-2}\,K^{-1}\,km^{-1}\,s}$ [102,103]. We assume that the 21 cm optical depth is negligible for our Galactic latitude cuts. This assumption breaks down for $|b| \lesssim 10°$ [104], which is smaller than our latitude cut.

Analytic WNM distribution: As an alternative to the 21 cm map, we consider an analytic model for the WNM, with a density proportional to

$$f_{\mathrm{WNM}}(\boldsymbol{x}) \propto \mathrm{sech}^2\left(\frac{z}{400\ \mathrm{pc}}\right) \exp\left(-\frac{R}{3.5\ \mathrm{kpc}}\right), \quad (3)$$

where z is the height with respect to the disk and R is Galactocentric radius. This functional form reflects the fact that the WNM forms less significant substructure due to its high temperature, such that its distribution in the Solar neighborhood is well-approximated by a 400 pc scale height and a 3.5 kpc disk scale length [105].

The precise relationship between gas components and gas tracers is complex, where some gas components are covered by multiple tracers. In our modeling, we take the CO to trace the surplus of H_2 that is otherwise not accounted for by the dust tracer. We perform fits for two separate models, labeled *A* and *B*, which are summarized in Table I. Model *A* includes the 21 cm map but not the f_{WNM} map, and vice versa for model *B*. The crucial difference is that the gas tracers have an overlap in terms of the CNM HI component in model *A*, but not for model *B*. By comparing their respective results we can estimate the amount of total hydrogen, HI, and CO-dark H_2 in the CNM. Model *B* is expected to perform slightly worse in terms of a χ^2 statistic, since f_{WNM} does not capture any WNM substructures. For this reason it is also highly degenerate with other smooth components (the ICS and isotropic background, see below). However, this is not detrimental to our fit, as the purpose of model *B* is to extract more information about the dust-to-gas conversion factor of the CNM, for which the ignored WNM substructures have a negligible effect.

TABLE I. Gas components (top row) and the respective maps (left column) they are traced by in model *A* and model *B*.

		CO H_2	CNM H_2	CNM HI	WNM HI
Model *A*	CO	✓			
	Dust		✓	✓	
	21 cm			✓	✓
Model *B*	CO	✓			
	Dust		✓	✓	
	f_{WNM}				✓

We employ the canonical assumption that all gas phases are mixed with the same fraction of helium, constituting 38% of the hydrogen gas mass, with an additional 4% mass from heavier elements [106–108]. The γ-ray production per mass is approximately the same for π^0 while bremsstrahlung from heavier targets is slightly suppressed, as described in the Supplemental Material [26], Appendix D. In our model, we ignore the hot interstellar medium (HIM), which constitutes a subpercent contribution to the local gas density and, despite its large scale height, a small contribution to the total gas surface density [109]. The HIM lacks smaller scale spatial structure, so its contribution to the γ-ray sky is absorbed by other smooth γ-ray emission components (listed below), without affecting the normalizations of the cold gas in our fit.

Other γ-ray emission components.—While γ rays from π^0 decay and bremsstrahlung both trace Galactic gas, there are several mechanisms that do not depend on the gas density. First, Fermi-LAT observations include over 5000 point sources of both Galactic and extragalactic origin, including supernova remnants, pulsars, blazars, and star-forming galaxies. The large number of sources makes it difficult to model the intensity and spectrum of each independently. Thus, we use the default flux and spectra for each source reported in the 4FGL-DR2 catalog

[95,110]. This provides an accurate model for nonvariable sources. In contrast, we mask the bright and time-variable sources as discussed in the Supplemental Material [26], Appendix C2.

The second component is the isotropic γ-ray background, which is primarily produced by the subset of extragalactic sources that are too dim to be individually detected. It also includes a contribution from cosmic rays that are misidentified as γ rays by the Fermi-LAT. Because both extragalactic sources and cosmic rays are isotropic, the morphological template in each bin matches the Fermi-LAT exposure.

The final component is the ICS of starlight by relativistic electrons. Notably, the same electron population produces the ICS and the bremsstrahlung component discussed above. To calculate the convolution of this electron distribution with Galactic radiation, we utilize the CR model described in the Supplementary Material [26], Appendix B, and the up-to-date interstellar radiation field models given by Ref. [89].

Fitting procedure.—We infer our results in a Bayesian framework, with a Poisson count data likelihood and flat box priors on the normalizations of each respective γ-ray map component, and sample the posterior probability density using Hamiltonian Monte-Carlo sampling. We produce our main results in a joint fit of the 4th–15th energy bin (0.4–100 GeV), which are dominated by hadronic interactions and therefore they are less prone to systematic errors related to bremsstrahlung cross sections, as well as Fermi's angular resolution, which improves at high energies. We employ jackknife subsampling by splitting the sky into sub-areas in order to quantify systematic uncertainties, and also perform fits for each separate γ-ray energy bin. See the Supplemental Material [26], Appendix D for further details.

Because we focus our analysis on the local ISM, we exclude regions of the sky where the γ-ray data include significant systematic uncertainties due to distant sources. These include (1) regions along the Galactic plane with $|b| < 16°$; (2) regions near the Galactic center with $|l| < 60°$, which removes contamination from the Fermi bubbles [111] and Loop I [112]; (3) a 3° radius circle around 17 highly variable Fermi-LAT point sources, for which the quoted 4FGL fluxes may not produce proper flux estimates; and (4) a 5° radius circle surrounding the position of the Large Magellanic Cloud. The sizes of these masks are motivated by the Fermi-LAT point spread function, which has a 2.93° 68% containment region for our lowest energy bin.

Results.—In Fig. 3, we show a comparison between the data count and the best-fit model *A*, for a fit of the full nonmasked sky over the 4th–15th energy bins (for individual energy bins, see Supplemental Material [26], Appendix D. The higher energy bins have limited statistics, so the fit is mainly driven by roughly the 4th–7th energy bins. Our model provides an overall good description of the data. However, some structures are not fully captured by our model. The mean absolute relative difference between the model and data counts in the nonmasked region is 5.9% and 9.5% for models *A* and *B*, beyond what can be accounted for by statistical noise. Hence, our result is strongly dominated by systematic uncertainties, which we estimate by jackknife subsampling.

The main focus of our results concerns the dust conversion factors, as presented in Fig. 1. A more complete visual representation of our results, including the conversion factors for the 21 cm and CO maps and their energy dependence, can be found in the Supplemental Material [26], Appendix D. The dust-to-H conversion factors differ significantly between the model *A* and model *B* fits. This is expected, as the 21 cm map of model *A* traces CNM HI and thus overlaps with the dust map. However, despite the CNM HI already being accounted for, the dust map is still inferred to contribute significantly to the γ-ray sky in model *A*, with a dust-to-H conversion factor of $(2.31 \pm 0.75) \times 10^{21}$ mag^{-1} cm^{-2} (posterior mean and standard deviation). Thus the dust map must also trace a component that is not accounted for in the 21 cm or CO maps. We make the interpretation that this additional component is CO-dark H_2 mixed in with the CNM. For our model *B*, which does not include the 21 cm map, the dust map is interpreted to trace the totality of both CNM HI and CNM H_2, with a dust-to-H conversion factor of $(6.28 \pm 0.94) \times 10^{21}$ mag^{-1} cm^{-2}. By taking the dust conversion factor difference between model *A* and model *B*, we obtain the amount of CNM HI traced by dust, inferred to be $(3.97 \pm 0.48) \times 10^{21}$ mag^{-1} cm^{-2}. This difference has a smaller uncertainty than the individual conversion factors because we account for correlations in the jackknife subsampling. The relative uncertainties for the dust-to-H conversion factor is roughly 12%, on the same order of magnitude as the systematic errors seen in the model and data comparison of Fig. 3.

For model *A*, we infer a 21 cm conversion factor of $(1.816 \pm 0.153) \times 10^{18}$ cm^{-2} K^{-1} km^{-1} s, consistent with

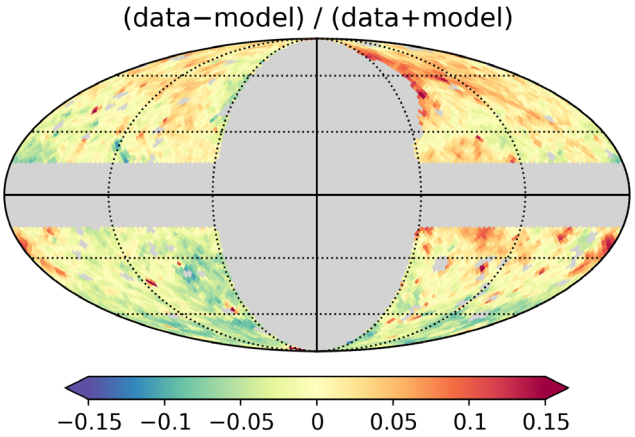

FIG. 3. Comparison of our model *A* with the data counts, from the best fit over the 4th–15th energy bins. Masked regions are gray.

the canonical value of 1.823×10^{18} cm^{-2} K^{-1} km^{-1} s [102,103]. This agreement is in general support of the accuracy of our analysis, and does not indicate any significant bias in for example the γ-ray cross sections. For the CO-to-H_2 conversion factor, we infer $(1.67 \pm 0.27) \times 10^{20}$ and $(0.81 \pm 0.45) \times 10^{20}$ cm^{-2} K^{-1} km^{-1} s for model *A* and *B*, respectively. These results for model *A* are consistent with the canonical value of $(2 \pm 0.6) \times 10^{20}$ cm^{-2} K^{-1} km^{-1} s. The CO-to-H_2 conversion factor discrepancy between model *A* and *B* implies that there is an overlap between the dust map and the CO map; in other words, the CO-bright H_2 is also in part traced by dust. The CO-to-H_2 conversion factor is potentially not very well understood [113], perhaps further complicated by its interplay with dust as a tracer. To investigate this in more detail would require a more extensive study, preferably including lower Galactic latitudes with a more significant CO signal.

Another important contribution to baryonic models for the Solar neighborhood is that we quantify the amount of CO-dark H_2 that is mixed with the CNM HI, to a mass fraction of $36.0 \pm 8.8\%$. This result agrees well with Ref. [25], which uses a completely different method affected by other systematic uncertainties (see Supplemental Material [26], Appendix A for details). Outside CO-bright regions, they find a CO-dark H_2 mass fraction of 46% relative to the total amount of hydrogen, although they do not state any uncertainty for this quantity.

We also perform additional tests, described in the Supplemental Material [26], Appendix D, for example, by applying an alternative data likelihood that is less sensitive to outliers. In summary, we obtain very similar results for these alternative fits, even with latitude cuts of $|b| > 12°$ and $|b| > 8°$, as well as at higher or lower angular resolution. Furthermore, in Supplemental Material [26], Appendix D5, we present a model for the cold gas mass density based on our results, and compare this model with estimates from other studies.

Conclusion.—We weigh the local ISM (within roughly 2 kpc), focusing on its cold gas components and, as a first work of its kind, do so using γ-ray data from Fermi-LAT and a dust map based on *Gaia* data. We employ a conservative treatment of uncertainties and potential systematic errors. Our results for the dust-to-gas conversion factor are robust and have sufficient precision to probe the range of results produced by current world-leading experiments. Furthermore, our method is highly complementary to these other studies, subject to different sources of potential systematic biases, and especially useful for revealing otherwise difficult to observe gas components such as CO-dark H_2.

This method for using γ rays to probe the ISM of the Solar neighborhood is expected to improve in the near future. The dust maps are getting deeper and more precise, due to better astrometric measurements from *Gaia*, complementary spectro- and photoastrometric distance information [114,115], and more sophisticated modeling of the three-dimensional distribution of dust (e.g., employing Gaussian processes [116,117]). Further improvements might be achieved by a better understanding and modeling of the cross sections for hadronic γ-ray production using the latest data from high-energy experiments.

We thank Adam Leroy, John Beacom, and Martin Rey for useful discussions. A. W. is supported by the Carlsberg Foundation via a Semper Ardens grant (CF15-0384). M. K. and T. L. are supported by the Swedish Research Council under Contract No. 2019-05135 and the European Research Council under Grant No. 742104. T. L. is also supported by the Swedish National Space Agency under Contract No. 117/19. This project used computing resources from the Swedish National Infrastructure for Computing (SNIC) under Projects No. 2021/3-42, No. 2021/6-326, and No. 2021-1-24 partially funded by the Swedish Research Council through Grant No. 2018-05973. This work made use of a HPC facility funded by a grant from VILLUM FONDEN (Project No. 16599). This work has made use of the following Python packages: NUMPY [118]; SCIPY [119]; TENSORFLOW [120]; PYMULTINEST [121]; IMINUIT [122]; MPI4PY [123].

*axel.widmark@nbi.ku.dk
†michael.korsmeier@fysik.su.se
‡linden@fysik.su.se

[1] J. I. Read, J. Phys. G **41**, 063101 (2014).
[2] P. F. de Salas and A. Widmark, Rep. Prog. Phys. **84**, 104901 (2021).
[3] P. R. Shapiro and G. B. Field, Astrophys. J. **205**, 762 (1976).
[4] A. Saintonge and B. Catinella, Annu. Rev. Astron. Astrophys. **60**, 319 (2022).
[5] M. Heyer and T. M. Dame, Annu. Rev. Astron. Astrophys. **53**, 583 (2015).
[6] A. D. Bolatto, M. Wolfire, and A. K. Leroy, Annu. Rev. Astron. Astrophys. **51**, 207 (2013).
[7] I. A. Grenier, J.-M. Casandjian, and R. Terrier, Science **307**, 1292 (2005).
[8] M. G. Wolfire, D. Hollenbach, and C. F. McKee, Astrophys. J. **716**, 1191 (2010).
[9] N. Tang, D. Li, C. Heiles, S. Wang, Z. Pan, and J.-J. Wang, Astron. Astrophys. **593**, A42 (2016).
[10] W. T. Reach, C. Heiles, and J.-P. Bernard, Astrophys. J. **834**, 63 (2017).
[11] B. T. Draine, Annu. Rev. Astron. Astrophys. **41**, 241 (2003).
[12] B. T. Draine and A. Li, Astrophys. J. **657**, 810 (2007).
[13] N. Scoville, H. Aussel, K. Sheth, K. S. Scott, D. Sanders, R. Ivison, A. Pope, P. Capak, P. Vanden Bout, S. Manohar, J. Kartaltepe, B. Robertson, and S. Lilly, Astrophys. J. **783**, 84 (2014).
[14] A. Rémy-Ruyer, S. C. Madden, F. Galliano, M. Galametz, T. T. Takeuchi, R. S. Asano, S. Zhukovska, V. Lebouteiller *et al.*, Astron. Astrophys. **563**, A31 (2014).

[15] K. D. Gordon, J. Roman-Duval, C. Bot, M. Meixner, B. Babler, J.-P. Bernard, A. Bolatto, M. L. Boyer *et al.*, Astrophys. J. **797**, 85 (2014).

[16] I. Lamperti, A. Saintonge, I. De Looze, G. Accurso, C. J. R. Clark, M. W. L. Smith, C. D. Wilson, E. Brinks *et al.*, Mon. Not. R. Astron. Soc. **489**, 4389 (2019).

[17] A. Saintonge, C. D. Wilson, T. Xiao, L. Lin, H. S. Hwang, T. Tosaki, M. Bureau, P. J. Cigan, C. J. R. Clark, D. L. Clements *et al.*, Mon. Not. R. Astron. Soc. **481**, 3497 (2018).

[18] R. S. Klessen and S. C. O. Glover, Saas-Fee Adv. Course **43**, 85 (2016).

[19] B. D. Savage, R. C. Bohlin, J. F. Drake, and W. Budich, Astrophys. J. **216**, 291 (1977).

[20] R. C. Bohlin, B. D. Savage, and J. F. Drake, Astrophys. J. **224**, 132 (1978).

[21] J. M. Shull, C. W. Danforth, and K. L. Anderson, Astrophys. J. **911**, 55 (2021).

[22] P. Predehl and J. H. M. M. Schmitt, Astron. Astrophys. **293**, 889 (1995).

[23] H. Liszt, Astrophys. J. **780**, 10 (2013).

[24] D. Lenz, B. S. Hensley, and O. Doré, Astrophys. J. **846**, 38 (2017).

[25] P. M. W. Kalberla, J. Kerp, and U. Haud, Astron. Astrophys. **639**, A26 (2020).

[26] See Supplemental Material at http://link.aps.org/supplemental/10.1103/PhysRevLett.130.161002 for further details on previous similar studies, our cosmic ray and γ-ray modelling, and additional results and figures; the Supplementary Material includes Appendices A–D and Refs. [27–82].

[27] D. J. Schlegel, D. P. Finkbeiner, and M. Davis, Astrophys. J. **500**, 525 (1998).

[28] G. Neugebauer, H. Habing, R. van Duinen, H. Aumann, B. Baud, C. Beichman, D. Beintema, N. Boggess *et al.*, Astrophys. J. Lett. **278**, L1 (1984).

[29] R. F. Silverberg, M. G. Hauser, N. W. Boggess, T. J. Kelsall, S. H. Moseley, and T. L. Murdock, in *Infrared Spaceborne Remote Sensing*, Society of Photo-Optical Instrumentation Engineers (SPIE) Conference Series Vol. 2019, edited by M. S. Scholl (SPIE, San Diego, 1993), pp. 180–189.

[30] K. Yahata, A. Yonehara, Y. Suto, E. Turner, T. Broadhurst, and D. Finkbeiner, Publ. Astron. Soc. Jpn. **59**, 205 (2007).

[31] E. F. Schlafly, G. Green, D. P. Finkbeiner, H. W. Rix, E. F. Bell, W. S. Burgett, K. C. Chambers, P. W. Draper *et al.*, Astrophys. J. **786**, 29 (2014).

[32] M. Korsmeier and A. Cuoco, Phys. Rev. D **105**, 103033 (2022).

[33] N. Weinrich, M. Boudaud, L. Derome, Y. Genolini, J. Lavalle, D. Maurin, P. Salati, P. Serpico, and G. Weymann-Despres, Astron. Astrophys. **639**, A74 (2020).

[34] L. O. Drury and A. W. Strong, Astron. Astrophys. **597**, A117 (2017).

[35] L. Derome, D. Maurin, P. Salati, M. Boudaud, Y. Génolini, and P. Kunzé, Astron. Astrophys. **627**, A158 (2019).

[36] M. Aguilar *et al.* (AMS Collaboration), Phys. Rep. **894**, 1 (2021).

[37] M. Korsmeier and A. Cuoco, Phys. Rev. D **94**, 123019 (2016).

[38] N. Tomassetti, Phys. Rev. D **96**, 103005 (2017).

[39] W. Liu, Y.-h. Yao, and Y.-Q. Guo, Astrophys. J. **869**, 176 (2018).

[40] Y. Génolini *et al.*, Phys. Rev. D **99**, 123028 (2019).

[41] C. Evoli, R. Aloisio, and P. Blasi, Phys. Rev. D **99**, 103023 (2019).

[42] C. Evoli, G. Morlino, P. Blasi, and R. Aloisio, Phys. Rev. D **101**, 023013 (2020).

[43] M. J. Boschini *et al.*, Astrophys. J. Suppl. Ser. **250**, 27 (2020).

[44] P. D. L. T. Luque, M. N. Mazziotta, F. Loparco, F. Gargano, and D. Serini, J. Cosmol. Astropart. Phys. 07 (2021) 010.

[45] P. De La Torre Luque, M. N. Mazziotta, F. Loparco, F. Gargano, and D. Serini, J. Cosmol. Astropart. Phys. 03 (2021) 099.

[46] B. Schroer, C. Evoli, and P. Blasi, Phys. Rev. D **103**, 123010 (2021).

[47] M.-J. Zhao, K. Fang, and X.-J. Bi, Phys. Rev. D **104**, 123001 (2021).

[48] B. Coste, L. Derome, D. Maurin, and A. Putze, Astron. Astrophys. **539**, A88 (2012).

[49] J. Wu and H. Chen, Phys. Lett. B **789**, 292 (2019).

[50] M. Aguilar *et al.* (AMS Collaboration), Phys. Rev. Lett. **120**, 021101 (2018).

[51] L. Derome, ICRC2021 (2021), https://video.desy.de/video/Cosmic-Ray-Isotopes-with-the-Alpha-Magnetic-Spectrometer/c1e42f1de4cdb29069278dffd612add1.

[52] Y. Genolini, D. Maurin, I. V. Moskalenko, and M. Unger, Phys. Rev. C **98**, 034611 (2018).

[53] L. A. Fisk, Astrophys. J. **206**, 333 (1976).

[54] D. A. Green, Mon. Not. R. Astron. Soc. **454**, 1517 (2015).

[55] D. R. Lorimer, IAU Symp. **218**, 105 (2004).

[56] D. Hooper, P. Blasi, and P. D. Serpico, J. Cosmol. Astropart. Phys. 01 (2009) 025.

[57] M. Aguilar *et al.* (AMS Collaboration), Phys. Rev. Lett. **114**, 171103 (2015).

[58] E. C. Stone, A. C. Cummings, F. B. McDonald, B. C. Heikkila, N. Lal, and W. R. Webber, Science **341**, 150 (2013).

[59] M. Aguilar *et al.* (AMS Collaboration), Phys. Rev. Lett. **119**, 251101 (2017).

[60] M. Aguilar *et al.* (AMS Collaboration), Phys. Rev. Lett. **123**, 181102 (2019).

[61] M. Aguilar *et al.* (AMS Collaboration), Phys. Rev. Lett. **117**, 091103 (2016).

[62] M. Aguilar *et al.* (AMS Collaboration), Phys. Rev. Lett. **113**, 121102 (2014).

[63] M. Aguilar *et al.* (AMS Collaboration), Phys. Rev. Lett. **122**, 041102 (2019).

[64] F. Feroz, M. P. Hobson, and M. Bridges, Mon. Not. R. Astron. Soc. **398**, 1601 (2009).

[65] F. Acero *et al.* (Fermi-LAT Collaboration), Astrophys. J. Suppl. Ser. **223**, 26 (2016).

[66] R. Yang, F. Aharonian, and C. Evoli, Phys. Rev. D **93**, 123007 (2016).

[67] M. Pothast, D. Gaggero, E. Storm, and C. Weniger, J. Cosmol. Astropart. Phys. 10 (2018) 045.

[68] M. Ajello *et al.* (Fermi-LAT Collaboration), Astrophys. J. **819**, 44 (2015).

[69] E. Carlson, T. Linden, and S. Profumo, Phys. Rev. D **94**, 063504 (2016).
[70] N. Bissantz, V. P. Debattista, and O. Gerhard, Astrophys. J. Lett. **601**, L155 (2004).
[71] M. Pohl, P. Englmaier, and N. Bissantz, Astrophys. J. **677**, 283 (2008).
[72] P. Mertsch and V. H. M. Phan, Astron. Astrophys. **671**, A54 (2023).
[73] S. Abdollahi *et al.* (Fermi-LAT Collaboration), Astrophys. J. Suppl. Ser. **260**, 53 (2022).
[74] T. Kamae, T. Abe, and T. Koi, Astrophys. J. **620**, 244 (2005).
[75] T. Kamae, N. Karlsson, T. Mizuno, T. Abe, and T. Koi, Astrophys. J. **647**, 692 (2006); **662**, 779(E) (2007).
[76] T. Sjostrand, L. Lonnblad, and S. Mrenna, arXiv:hep-ph/0108264.
[77] M. Kachelrieß, I. V. Moskalenko, and S. Ostapchenko, Comput. Phys. Commun. **245**, 106846 (2019).
[78] S. Ostapchenko, Phys. Rev. D **83**, 014018 (2011).
[79] I. V. Moskalenko and A. W. Strong, Astrophys. J. **493**, 694 (1998).
[80] S. A. Stephens and G. D. Badhwar, Astrophys. Space Sci. **76**, 213 (1981).
[81] B. Efron, *The Jackknife, the Bootstrap and Other Resampling Plans* (Society for Industrial and Applied Mathematics, Philadelphia, 1982).
[82] K. Schutz, T. Lin, B. R. Safdi, and C.-L. Wu, Phys. Rev. Lett. **121**, 081101 (2018).
[83] R. Lallement, C. Babusiaux, J. L. Vergely, D. Katz, F. Arenou, B. Valette, C. Hottier, and L. Capitanio, Astron. Astrophys. **625**, A135 (2019).
[84] Gaia Collaboration, Astron. Astrophys. **616**, A1 (2018).
[85] The templates are made available upon request.
[86] M. Ackermann *et al.* (Fermi-LAT Collaboration), Astrophys. J. **750**, 3 (2012).
[87] M. Ackermann *et al.* (Fermi-LAT Collaboration), Astrophys. J. **799**, 86 (2015).
[88] L. Tibaldo, D. Gaggero, and P. Martin, Universe **7**, 141 (2021).
[89] T. A. Porter, G. Johannesson, and I. V. Moskalenko, Astrophys. J. **846**, 67 (2017).
[90] G. Jóhannesson, T. A. Porter, and I. V. Moskalenko, Astrophys. J. **856**, 45 (2018).
[91] R. Kissmann, F. Niederwanger, O. Reimer, and A. W. Strong, AIP Conf. Proc. **1792**, 070011 (2017).
[92] A. Dundovic, C. Evoli, D. Gaggero, and D. Grasso, Astron. Astrophys. **653**, A18 (2021).
[93] M. Korsmeier and A. Cuoco, Phys. Rev. D **103**, 103016 (2021).
[94] A. Strong, I. Moskalenko, and O. Reimer, Astrophys. J. **537**, 763 (2000); **541**, 1109(E) (2000).
[95] S. Abdollahi *et al.* (Fermi-LAT Collaboration), Astrophys. J. Suppl. Ser. **247**, 33 (2020).
[96] C. F. McKee and J. P. Ostriker, Astrophys. J. **218**, 148 (1977).
[97] D. P. Cox, Annu. Rev. Astron. Astrophys. **43**, 337 (2005).
[98] B. T. Draine, *Physics of the Interstellar and Intergalactic Medium* (Princeton University Press, Princeton, 2011).
[99] Planck Collaboration, Astron. Astrophys. **571**, A13 (2014).
[100] R. L. Dickman, Astrophys. J. Suppl. Ser. **37**, 407 (1978).
[101] G. M. Green, E. Schlafly, C. Zucker, J. S. Speagle, and D. Finkbeiner, Astrophys. J. **887**, 93 (2019).
[102] HI4PI Collaboration, Astron. Astrophys. **594**, A116 (2016).
[103] T. L. Wilson, K. Rohlfs, and S. Hüttemeister, *Tools of Radio Astronomy* (Springer, Berlin, 2009).
[104] C. Murray, S. Stanimirović, W. Goss, C. Heiles, J. Dickey, B. Babler, and C.-G. Kim, Astrophys. J. Suppl. Ser. **238**, 14 (2018).
[105] P. M. W. Kalberla and J. Kerp, Annu. Rev. Astron. Astrophys. **47**, 27 (2009).
[106] L. Bronfman, R. S. Cohen, H. Alvarez, J. May, and P. Thaddeus, Astrophys. J. **324**, 248 (1988).
[107] K. M. Ferrière, Rev. Mod. Phys. **73**, 1031 (2001).
[108] E. D. Kramer and L. Randall, Astrophys. J. **829**, 126 (2016).
[109] C. F. McKee, A. Parravano, and D. J. Hollenbach, Astrophys. J. **814**, 13 (2015).
[110] J. Ballet, T. H. Burnett, S. W. Digel, and B. Lott (Fermi-LAT Collaboration), arXiv:2005.11208.
[111] M. Su, T. R. Slatyer, and D. P. Finkbeiner, Astrophys. J. **724**, 1044 (2010).
[112] J.-M. Casandjian and I. Grenier, arXiv:0912.3478.
[113] S. C. O. Glover and M. M. Mac Low, Mon. Not. R. Astron. Soc. **412**, 337 (2011).
[114] C. A. L. Bailer-Jones, J. Rybizki, M. Fouesneau, M. Demleitner, and R. Andrae, Astrophys. J. **161**, 147 (2021).
[115] F. Anders, A. Khalatyan, A. B. A. Queiroz, C. Chiappini, J. Ardèvol, L. Casamiquela, F. Figueras, Ó. Jiménez-Arranz *et al.*, Astron. Astrophys. **658**, A91 (2022).
[116] A. C. Miller, L. Anderson, B. Leistedt, J. P. Cunningham, D. W. Hogg, and D. M. Blei, arXiv:2202.06797.
[117] R. H. Leike, G. Edenhofer, J. Knollmüller, C. Alig, P. Frank, and T. A. Enßlin, arXiv:2204.11715.
[118] C. R. Harris *et al.*, Nature (London) **585**, 357 (2020).
[119] P. Virtanen *et al.* (SciPy 1.0 Contributors), Nat. Methods **17**, 261 (2020).
[120] M. Abadi *et al.*, TensorFlow: Large-scale machine learning on heterogeneous systems (2015), tensorflow.org.
[121] J. Buchner, PyMultiNest: Python interface for MultiNest, Astrophysics Source Code Library, record ascl:1606.005 (2016), ascl:1606.005.
[122] H. Dembinski *et al.* (2020), 10.5281/zenodo.3949207.
[123] L. Dalcín, R. Paz, and M. Storti, J. Parallel Distrib. Comput. **65**, 1108 (2005).